Electron. Mater. Lett., Vol. 11, No. 2 (2015), pp. 193-197
DOI: 10.1007/s13391-014-4223-2

Structure, Morphology, and Optical Properties of $(Ca_{1-3x}Eu_{2x})WO_4$ Microcrystals

R. F. Gonçalves,[1] M. J. Godinho,[2] A. P. A. Marques,[1] M. R. C. Santos,[2] I. L. V. Rosa,[4] E. Longo,[3] M. Siu Li,[5] J. L. S. Sa,[6] and L. S. Cavalcante[6,*]

[1]Universidade Federal de São Paulo, Diadema, São Paulo 09972-270, Brazil
[2]Departamento de Química-CAC, Universidade Federal de Goiás, Catalão, Goiás 75704-020, Brazil
[3]LIEC-IQ-Universidade Estadual Paulista, Araraquara, São Paulo 14801-907, Brazil
[4]LIEC-DQ-Universidade Federal de São Carlos, São Carlos, São Paulo 13565-905, Brazil
[5]IFSC-Universidade de São Paulo, P.O. Box 369, 13560-970, São Carlos, SP, Brazil
[6]CCN-DQ-GERATEC, Universidade Estadual do Piauí, Teresina, Piauí 64002-150, Brazil

(received date: 3 August 2014 / accepted date: 15 October 2014 / published date: 10 March 2015)

In this letter, we report the efficient, surfactant-free, microwave-hydrothermal method of synthesizing calcium europium tungstate [$(Ca_{1-3x}Eu_{2x})WO_4$, x = 0, 0.05, 0.01, 0.02, and 0.04] microcrystals. The structure and morphology were investigated using X-ray diffraction (XRD), Fourier-transform Raman (FT-Raman) spectroscopy, and field emission scanning electron microscopy (FE-SEM). XRD patterns and FT-Raman spectra indicated that all $(Ca_{1-3x}Eu_{2x})WO_4$ microcrystals has a scheelite-type tetragonal structure. FE-SEM images revealed that the Eu^{3+} ions systematically affect the crystal shape and that there are two different types of superstructures: rice- and dumbbell-like microcrystals. The photoluminescence emission of the doped microcrystals changed relative to that of pure $CaWO_4$ owing to the presence of defects and new energy levels associated with the Eu^{3+} content, which promotes the appearance of intermediate electronic levels in the band gap.

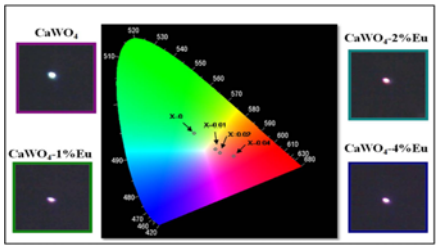

Keywords: $CaWO_4$, microcrystals, europium, microwave, Raman, photoluminescence

1. INTRODUCTION

Tungstate crystals formed with alkaline earth metals as network modifiers, with the general formula (AWO_4, A = Ca, Sr, and Ba),[1-3] are important members of inorganic oxide families having a scheelite-type tetragonal structure and space group ($I4_1/a$).[4] Among these tungstate crystals, that of calcium ($CaWO_4$) has been widely investigated owing to its unique structure, good chemical and physical stability, microwave dielectric characteristic, strong visible luminescence, and thermoluminescence properties.[5-8]

Several synthetic routes for the preparation of $CaWO_4$ crystals and thin films have been reported in the literature, such as molten salt,[9] chemical solution,[10] galvanic cell,[11] solid-state reaction,[12] hydrothermal,[13] and microwave-assisted hydrothermal (MAH)[14] methods. Among these, the conventional hydrothermal (CH) method is an excellent route to obtain crystalline oxides of different materials. However, the main drawback of this method is the associated slow crystallization kinetics of material oxides, requiring 12 - 48 h of processing.[15,16] Komarneni *et al.*[17,18] solved the problems of thermal gradients and slow reaction kinetics of the CH method by implementing microwave radiation as an energy source. The resulting method, called microwave-hydrothermal (MH), was able to reduce the processing time from a few hours to a few minutes and increase the level of oxide crystallization.[19] These improvements of MH over CH arise from the direct interaction of microwaves with ions or molecules in a solution or with solid phases dispersed in a liquid medium. In fact, it is important to highlight that the efficiency of the microwave-thermal energy conversion is governed by the following physical variables: tangent loss, relaxation time, and penetration depth.[20] Moreover, previous reports show that structural changes and the introduction of dopants in the A-sites via

*Corresponding author: laeciosc@bol.com.br

doping with rare earth ions (RE^{3+} = Sm^{3+}, Tb^{3+}, Dy^{3+}) can form $CaWO_4$ crystals with diverse physical and chemical properties, as well as a few new optical properties such as photoluminescence and red phosphors.[21-25]

Therefore, in this letter, we report the successful synthesis of a series of $(Ca_{1-3x}Eu_{2x})WO_4$ microcrystals, with Eu^{3+} mol ratio $x = 0$, 0.005, 0.01, 0.02, and 0.04, through the surfactant-free MH method. Moreover, structural characterization was performed with X-ray diffraction (XRD) and Fourier-transform Raman (FT-Raman) spectroscopy. Morphological aspects were investigated using field emission scanning electron microcopy (FE-SEM) images. Finally, optical properties were determined by ultraviolet-visible (UV-vis) diffuse reflectance spectroscopy and photoluminescence (PL) measurement at room temperature.

2. EXPERIMENTAL PROCEDURE

$(Ca_{1-3x}Eu_{2x})WO_4$ microcrystals were synthesized through the coprecipitation method[4] without surfactants in aqueous solution at room temperature. A white precipitate powder was obtained from the stoichiometric mixture of tungstate (VI) sodium dihydrate ($Na_2WO_4{\cdot}2H_2O$) (99% purity, Sigma-Aldrich) and calcium (II) acetate monohydrate [$Ca(CH_3COO)_2{\cdot}H_2O$] (99% purity, Aldrich) in aqueous solution. Europium (III) oxide (Eu_2O_3) (99.999% purity, Aldrich) was employed as the Eu source. The mixture containing all ions involved was homogenized and transferred to a sealed Teflon autoclave and placed in a 2.45-GHz MH system with a maximum power of 800 W. The reaction mixture was heated at 130°C for 30 min. Thereafter, the autoclave was cooled naturally to room temperature. The product was subsequently washed several times to a neutral pH and dried at 50°C for 6 h. The obtained crystals were structurally characterized by XRD using a Shimadzu XRD-6000 (Japan) with Cu-Kα radiation ($\lambda = 1.5406$ Å). The FT-Raman spectra were recorded with a Bruker RFS 100 (Germany). The morphologies of the $(Ca_{1-3x}Eu_{2x})WO_4$ crystals were observed by FE-SEM using a Carl Zeiss Supra 35-VP (Germany) operated at 6 kV. PL measurements were performed at room temperature using a Monospec 27 monochromator coupled to a R446 photomultiplier (Hamamatsu, Japan). A krypton ion laser (Coherent Innova 90K, USA) ($\lambda = 350$ nm) was used as the excitation source; its maximum output power was maintained at 500 mW.

3. RESULTS AND DISCUSSION

3.1 Analyses of XRD patterns and FT-Raman spectra

Figures 1(a,b) show the XRD patterns and FT-Raman spectra, respectively, of the $(Ca_{1-3x}Eu_{2x})WO_4$ crystals obtained through the MH method at 130°C for 30 min.

In Fig. 1(a), all diffraction peaks are exactly indexed to the

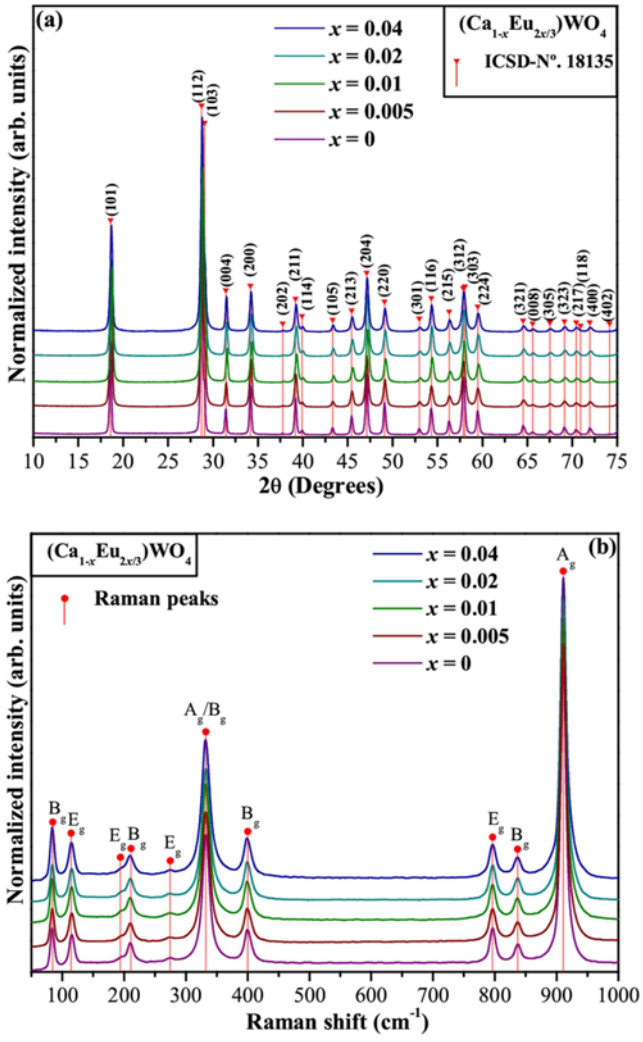

Fig. 1. (a) XRD patterns and (b) FT-Raman spectra of $(Ca_{1-3x}Eu_{2x})WO_4$ microcrystals with x = (a) 0, (b) 0.005, (c) 0.01, (d) 0.02, and (e) 0.04.

scheelite-type tetragonal structure with the space group ($I4_1/a$) related to Inorganic Crystal Structure Database (ICSD) No. 18135.[26] Secondary phases are not observed in the diffractograms, revealing that the MH treatment can promote pure phase formation.

Moreover, the presence of strong, sharp diffraction peaks is a typical characteristic of materials with a long-range structural order. The FT-Raman spectra in Fig. 1(b) indicate that 11 active Raman modes have the same frequencies before and after the replacement of Ca^{2+} with Eu^{3+} ions.[27] The positions and shapes of each peak are almost identical with those recorded in the literature, which indicate that the $(Ca_{1-3x}Eu_{2x})WO_4$ microcrystals are structurally ordered at short range with strong interaction between clusters arising from the symmetric stretching (←O←W→O→).

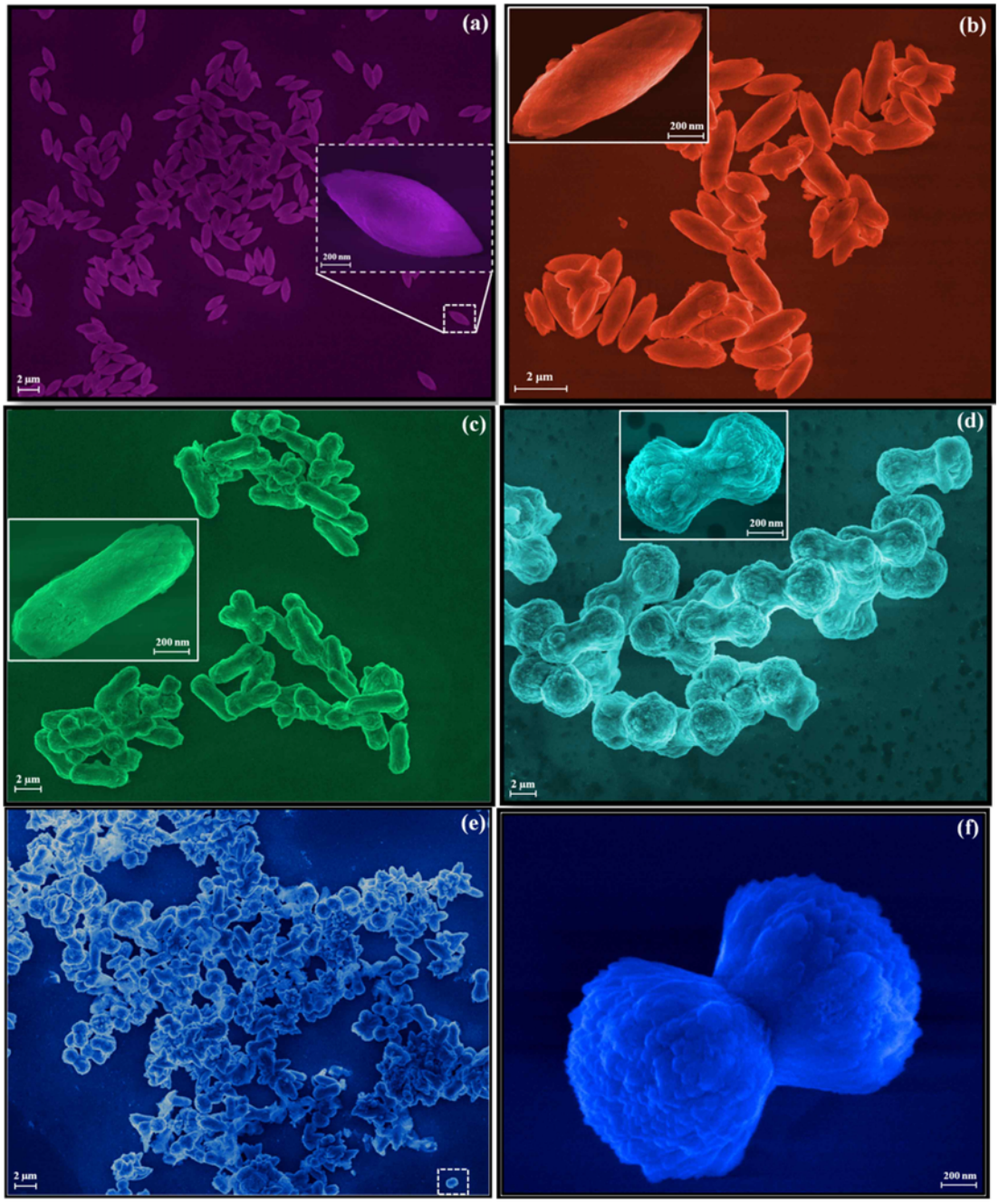

Fig. 2. FE-SEM images of $(Ca_{1-3x}Eu_{2x})WO_4$ microcrystals with x = (a) 0, (b) 0.005, (c) 0.01, (d) 0.02, and (e,f) 0.04.

3.2 FE-SEM analyses

Figures 2(a-f) show the FE-SEM images of the $(Ca_{1-3x}Eu_{2x})WO_4$ crystals at various x.

The FE-SEM images are of fundamental importance toward understanding the structural evolution of $CaWO_4$ microcrystals with the substitution of Ca^{2+} by Eu^{3+} ions. Figure 2(a) shows a large quantity of rice-like microcrystals for pure $CaWO_4$. These superstructures are composed of aggregated nanocrystals, as can be seen in the individual $CaWO_4$ microcrystal shown in the inset of Fig. 2(a). These crystals are formed by the self-assembly of several nanocrystals partially oriented with each other and have an average size of approximately 2.4 μm. Figure 2(c) clearly shows that with further substitution of Ca^{2+} by Eu^{3+} ions, the crystals expand at both ends with a slight shrinkage at the center. The division of a large crystal into two smaller spherical ones becomes more evident at a higher percentage of Eu^{3+} ions (x = 0.02 and 0.04) in the $CaWO_4$ crystal matrix, as can be

seen in Figs. 2(d,e) and the inset of Fig. 2(f). These crystals have an average size of approximately 1.5 and 1.2 μm, respectively. To minimize the overall system energy, a significant number of these seed particles tend to aggregate.[28,29]

3.3 PL emission analyses and Commission Internationale de l'Eclaira (CIE) chromaticity coordinates

The PL emission spectra of pure $CaWO_4$ consist of a strong and broad band from 350 to 750 nm, with the maximum emission at 525 nm (Fig. 3(a)). This sample shows PL emission in the blue-green spectral region, which is typical of a multiphonon process, i.e., system relaxation occurs through various paths involving the participation of numerous states. The PL properties of the pure material are directly related to the degree of structural order-disorder.

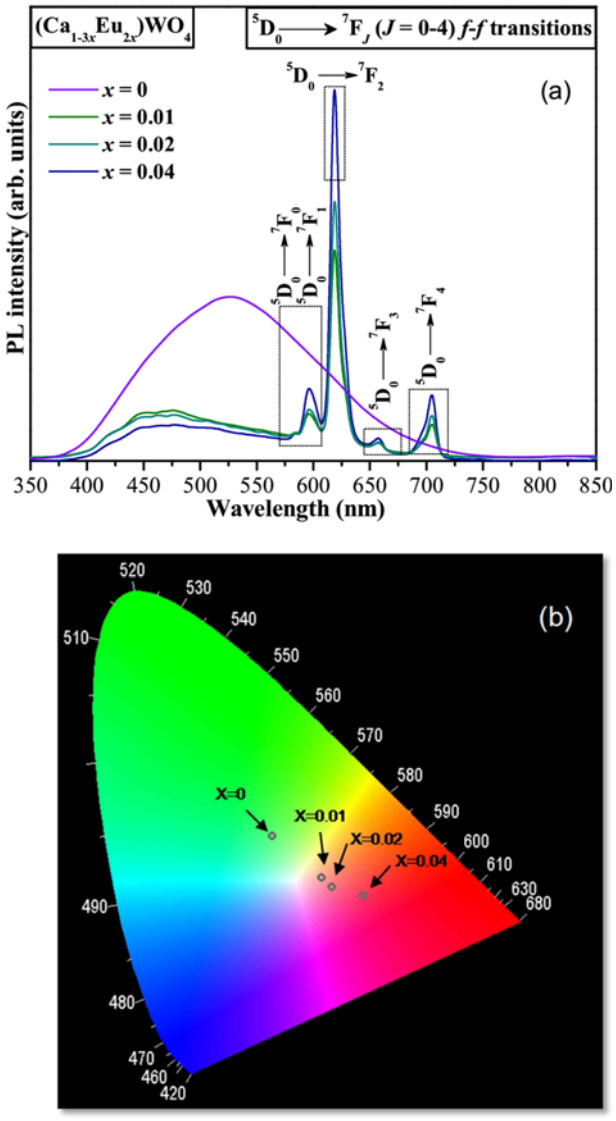

Fig. 3. (a) PL emission and (b) CIE chromaticity coordinates of $(Ca_{1-3x}Eu_{2x})WO_4$ microcrystals with $x = 0$, 0.01, 0.02, and 0.04.

When Eu^{3+} was introduced into pure $CaWO_4$, three Ca^{2+} sites were substituted by two Eu^{3+} neighbors to maintain electrical neutrality, and the composition of $(Ca_{1-3x}Eu_{2x})WO_4$ changed from $x = 0.01$ to 0.04. PL is strongly dependent on the Eu^{3+} content because its addition leads to a change in defects or the order-disorder of materials. The intensity of the PL emission changes with the introduction of the dopant, as indicated in (Fig. 3(a)). The PL emission spectra of Eu^{3+}-doped crystals show a reduction in the wide band and the appearance of a narrow band corresponding to *f-f* transitions in Eu^{3+}.[30] As the Eu^{3+} concentration in the $CaWO_4$ lattice increases, the PL emission of the host matrix becomes more suppressed while that of the Eu^{3+} ion prevails. Thus, in this wavelength range, loss of energy (non-radiative lattice vibrations) probably promotes PL suppression in the host matrix.

According to Fig. 3(a), the doped $CaWO_4$ presents a predominant red emission, characteristic of the $^5D_0 \rightarrow {}^7F_2$ transition in Eu^{3+}. The $(Ca_{1-3x}Eu_{2x})WO_4$ microcrystals with $x = 0.01$-0.04 display intense red-light emission at around 618 nm. The emission spectra of all samples present peaks at 582, 595, 618, 656, and 705 nm ascribed to the $^5D_0 \rightarrow {}^7F_J$ transition in Eu^{3+}, with $J = 0$, 1, 2, 3, and 4, respectively. The intensity of the $^5D_0 \rightarrow {}^7F_2$ transition, called hypersensitive, is strongly dependent on the surrounding Eu^{3+} owing to its electric dipole characteristic, while the $^5D_0 \rightarrow {}^7F_1$ transition has a magnetic dipole characteristic and its intensity is almost independent of the environment.

The CIE chromaticity coordinates are one of the important factors for evaluating the performance of the prepared phosphors. Therefore, the CIE chromaticity coordinate diagrams of $CaWO_4$:Eu^{3+} phosphors under 350 nm excitation were obtained using intensity-calibrated emission spectra data and the chromatic standard issued by the CIE, and shown in Fig. 3(b).

The chromaticity coordinates are (0.3097, 0.4116), (0.3934, 0.3400), (0.4115, 0.3238), and (0.4643, 0.3094) corresponding to Eu^{3+} compositions of $x = 0.0$, 0.01, 0.02, and 0.04, respectively. As shown in Fig. 3(b), the CIE chromaticity coordinates of the $CaWO_4$:Eu^{3+} crystals indicate that the coordinates of the pure $CaWO_4$ sample are located mostly in the blue-green region. Thus, as the Eu^{3+} concentration increases, the chromaticity coordinates of the samples gradually move toward the red (low-energy) region. For the $(Ca_{1-3x}Eu_{2x})WO_4$ sample with $x = 0.04$, the color coordinates are well fitted in the red region, corresponding to the $^5D_0 \rightarrow {}^7F_2$ transition in Eu^{3+} (618 nm). This behavior is consistent with the PL results presented in the emission spectra shown in Fig. 3(a).

4. CONCLUSIONS

In summary, we reported the facile synthesis of

$(Ca_{1-3x}Eu_{2x})WO_4$ microcrystals, with x = 0, 0.005, 0.01, 0.02, and 0.04, through the MH method. XRD patterns and FT-Raman spectra indicated that with the addition of Eu^{3+} ions, these crystals adopted a scheelite-type tetragonal structure without deleterious phases. The FE-SEM images revealed that in the absence of any surfactant or template, the introduction of Eu^{3+} ions led to a change in the crystal shape and reduction in the crystal size. The architectural control of nano- and microcrystals with well-defined shapes is an important goal of modern materials chemistry. The wide and narrow PL emission of $(Ca_{1-3x}Eu_{2x})WO_4$ microcrystals corresponding to *p–d* transitions in the pure material and 4*f*–4*f* internal transitions, respectively, is due to Eu^{3+} ions.

ACKNOWLEDGEMENTS

The authors acknowledge the financial support of the following Brazilian research funding institutions: FAPESP 2013/07296-2, INCTMN 2008/57872-1, CNPq (573636/2008-7, 304531/2013-8), and CAPES.

REFERENCES

1. S. Basu, B. S. Naidu, B. Viswanadh, V. Sudarsan, S. N. Jha, D. Bhattacharyya, and R. K. Vatsa, *RSC Adv.* **4**, 15606 (2014).
2. L. S. Cavalcante, J. C. Sczancoski, N. C. Batista, E. Longo, J. A. Varela, and M. O. Orlandi, *Adv. Powder Technol*. **24**, 344 (2013).
3. A. Singh, D. P. Dutta, J. Ramkumar, K. Bhattacharya, A. K. Tyagi, and M. H. Fulekar, *RSC Adv.* **3**, 22580 (2013).
4. L. S. Cavalcante, V. M. Longo, J. C. Sczancoski, M. A. P. Almeida, A. A. Batista, J. A. Varela, M. O. Orlandi, E. Longo, and M. S. Li, *Cryst. Eng. Comm*. **14**, 853 (2012).
5. L. Cheng, P. Liu, S.-X. Qu, and H. W. Zhang, *J. Alloys Compd*. **581**, 553 (2013).
6. L. Wang and J. J. Bian, *Mater. Lett*. **65**, 726 (2011).
7. Y. Li, Z. Wang, L. Sun, Z. Wang, S. Wang, X. Liu, and Y. Wang, *Mater. Res. Bull*. **50**, 36 (2014).
8. K. G. Sharma, N. S. Singh, Y. R. Devi, N. R. Singh, and S. D. Singh, *J. Alloys Compd*. **556**, 94 (2013).
9. Y. Wang, J. Ma, J. Tao, X. Zhu, J. Zhou, Z. Zhao, L. Xie, and H. Tian, *Mater. Lett*. **60**, 291 (2006).
10. M. A. M. A. Maurera, A. G. Souza, L. E. B. Soledade, F. M. Pontes, E. Longo, E. R. Leite, and J. A. Varela, *Mater. Lett*. **58**, 727 (2004).
11. C. Cui, J. Bi, and D. Gao, *Mater. Lett*. **62**, 2222 (2008).
12. F. Liang, Y. Hu, L. Chen, and X. Wang, *Appl. Phys. A* **115**, 859 (2014).
13. S. Liu, S. Tian, and R. Xing, *Cryst. Eng. Comm*. **13**, 7285 (2011).
14. V. M. Longo, L. Gracia, D. G. Stroppa, L. S. Cavalcante, M. Orlandi, A. J. Ramirez, E. R. Leite, J. Andres, A. Beltran, J. A. Varela, and E. Longo, *J. Phys. Chem. C*. **115**, 20113 (2011).
15. J. Deng, L. Chang, P. Wang, E. Zhang, J. Ma, and T. Wang, *Cryst. Res. Technol*. **47**, 1004 (2012).
16. H. Dong, Z. Li, Z. Ding, H. Pan, X. Wang, and X. Fu, *Sensors and Actuators B*. **140**, 623 (2009).
17. S. Komarneni and R. Roy, *Mater. Lett*. **4**, 107 (1986).
18. S. Komarneni and R. Roy, *Mater. Res. Bull*. **27**, 13963 (1992).
19. L. S. Cavalcante, J. C. Sczancoski, R. L. Tranquilin, J. A. Varela, E. Longo, and M. O. Orlandi, *Particuology* **7**, 353 (2009).
20. G. J. Wilson, A. S. Matijasevich, D. R. G. Mitchell, J. C. Schulz, and G. D. Will, *Langmuir*. **22**, 2016 (2006).
21. H. Y. He and Y. Wang, *J. Mater. Sci.: Mater. Electron*. **24**, 4847 (2013).
22. M. Wang, Y. Shi, Y. Tang, and G. Jiang, *Mater. Lett*. **109**, 12 (2013).
23. K. G. Sharma and N. R. Singh, *New J. Chem*. **37**, 2784 (2013).
24. X. Lou and D. Chen, *Mater. Lett*. **62**, 1681 (2008).
25. Y. Su, L. Li, and G. Li, *Chem. Mater*. **20**, 6060 (2008).
26. R. D. Burbank, *Acta Crystallogr*. **18**, 88 (1965).
27. Y. Chen, S. W. Park, B. K. Moon, B. C. Choi, J. H. Jeong, and C. Guo, *Cryst. Eng. Comm*. **15**, 8255 (2013).
28. V. S. Marques, L. S. Cavalcante, J. C. Sczancoski, A. F. P. Alcântara, M. O. Orlandi, E. Moraes, E. Longo, J. A. Varela, M. S. Li, and M. R. M. C. Santos, *Crys. Growth Des*. **10**, 4752 (2010).
29. R. F. Gonçalves, J. T. O. Figueiredo, A. T. de Figueiredo, M. S. Li, E. Longo, and M. J. Godinho, *Cryst. Eng. Comm*. **15**, 3292 (2013).
30. Y. Chen, B. K. Moon, B. C. Choi, J. H. Jeong, and H. K. Yang, *J. Am. Ceram. Soc*. **96**, 3596 (2013).